



Evaluating the effectiveness of stay-in-place forms to improve the torsional stability of box beam bridges during erection

Karl E. Barth¹, Michael W. Seek², Gregory K. Michaelson³,
Dimitra Pyrialakou⁴, Brook T. Woldegabriel⁵

Abstract

Cold-formed tub girders provide an effective steel solution for short-span bridges. The girders are often delivered with an open top with stay-in-place forms installed on site. Walkways may be installed to the side of the girder that can induce significant torsion rotations in the open cross section. Full scale tests on girder specimens have shown that installing one or two panels of stay in place forms at the ends of the girder can significantly reduce the torsion rotation of the girder by providing warping resistance. Cantilever tests on the stay in place forms are performed to investigate the influence of different connection conditions and combinations of panels on the in-plane diaphragm stiffness of the forms. An analytical model is developed that predicts the warping resistance provided by stay in place forms as a function of the in-plane diaphragm stiffness. This model can thus be used to determine the required stay in place form conditions to limit torsional rotations of tub girders during erection.

1. Introduction

Press-break-formed tub girders (PBFTG) developed by the Short Span Steel Bridge Alliance provide a cost-effective solution for short span steel bridges (spans from 20 ft. (6 m) to nearly 100 ft (30.5 m)). These girders are formed from flat plate into a U-shape (or inverted hat-shape) as shown in Fig. 2 through a press-break process. The girder depth typically ranges from many range from 12 in. (305 mm) deep up to 36 in. (915 mm) deep with a corresponding girder width of approximately 4 ft (1220 mm). These girders are placed in parallel with spacing ranging from approximately 5 feet to 10 feet as necessary to provide the requisite strength and roadway width. Steel studs are welded to the top flanges of the girders to create a composite system once a concrete deck is placed on top of the girders. To facilitate the placement of the concrete deck, light gauge stay-in-place forms (SIP's) are placed between the flanges of each girder as well as between each girder as shown in Fig. 1.

¹ Associate Professor, West Virginia University, <karl.barth@mail.wvu.edu>

² Associate Professor, Old Dominion University, <mseek@odu.edu>

³ Associate Professor, Marshall University, <michaelson@marshall.edu>

⁴ Assistant Professor, West Virginia University, <dimitra.pyrialakou@mail.wvu.edu>

⁵ Structural Engineer, AECOM Technical Services, <btw0011@mix.wvu.edu>

These SIPs may be installed to the girder in the shop however to facilitate nesting and avoid potential damage to the SIP during transport, it is advantageous to ship the girders bare and install the SIPs in the field. The stability of these girders is of particular interest during erection. Unlike traditional I-shaped girders which are typically installed with diaphragms between to improve stability during erection and to help with load distribution, there is no direct connection between the adjacent tub girders except for the SIPs connect between. The SIPs provide partial laterally stability, however, pattern loading conditions during construction (loading of the SIP between the girders) can induce torsion effects on the girders. Additionally, the end girders may have temporary catwalks attached to the side of the girder to provide workers access to the length of the bridge during construction as shown in Fig. 1. These weight of the catwalk and the associated live load it supports can also induce torsion on the girders.

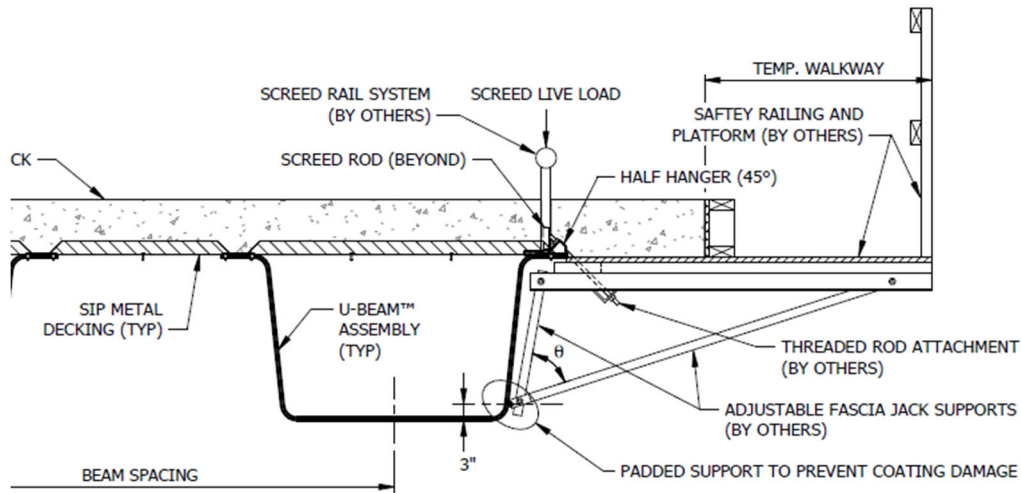


Figure 1 Tub girder construction detail with temporary walkway (Valmont, 2024).

Several failures have occurred during erection of both I-shaped girders and larger plate girder tub bridges due to inadequate bracing. Much of the bracing is only required during erection and the bracing details can significantly impact the cost of the girders (Wang et al, 2016), therefore understanding the behavior of girders during erection is essential. Heavier rolled structural sections have typically been used for the bracing of these girders and any capacity added by stay-in-place forms has typically been ignored. Sanchez and White (2012) studied various parameters of stay in place forms and their influence on the structural response of I-shaped girders. Egilmez et. al. (2016) investigated SIP connection details to I-girders and showed that with improved connections, SIPs could be used to effectively brace girders during construction. I-shapes have traditionally used an angle suspended from the top flange of I-girders to connect the SIPs between girders and this connection introduces the flexibility that renders the SIPs ineffective for bracing I-shaped girders. However, the practice with PBFTG's is to attach the SIPs directly to the top flanges, allowing the SIPs to directly transfer much of their stiffness to the tub girder. This, coupled with the fact that the stability demands of these smaller tub girders makes the potential for using SIPs for bracing much more attractive.

It is important therefore to understand the torsional behavior of these girders during erection to quantify the benefits provided by the SIPs. At the outset, it was logically expected that the addition

of the SIPs between the top flanges of the girder would increase the torsional resistance and reduce torsional rotation of the girder. Quantifying the torsional behavior serves as a starting point for establishing erection protocols and better define buckling capacities during erection. To better understand this behavior, full scale tests were performed on a single girder. The tests, discussed in Section 2, applied different combinations of SIPs to the top flange of the girder under different loading patterns and measured the torsional deformation of the specimen. Section 3 discusses the shell finite element models that were developed to validate the tests and provide a platform from which to perform additional parametric studies. Based on the behavior extracted from the finite element models, an analytical model is presented in Section 4 that predicts the restraining effect of the SIPs attached to the top flange of the girder.

2. Full scale torsion tests on girders

Full scale torsion tests were performed at West Virginia University to evaluate the torsional behavior of a press break formed tub girder. The girder was initially tested with no SIPs attached, then subsequent tests were performed with the addition of SIPs with different fastening patterns to evaluate the impact that adding the SIPs had on the torsional behavior.

2.1 Test Specimen

The specimen used for testing is a U18 cross section provided by Valmont Industries (Valmont, 2024). The cross section is 18 in. deep and 52 in. wide. See Fig. 2 for the dimensions of the cross section. The was fabricated from plate with a 3/8 in. thickness with ASTM A709 GR50 Steel.

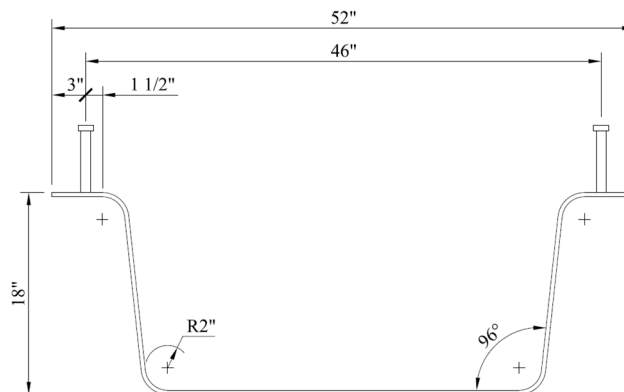


Figure 2 Tub Girder Cross section dimensions

As shown in Fig. 3, the overall length of the girder is 30 feet. Located at 3 in. from each end of the beam is a 3/8 in. thick diaphragm plate that is welded to the girder with single sided 1/4 in. fillet welds. This serves as the centerline of the bearing so the net span of the girder is 29 ft.-6 in. Along the length of the girder, five L4x4x1/4 angles are connected between the top flanges of the girder. The top leg of the angle is flush with the top flange of the girder and attached with a single bevel partial penetration weld. The other leg of the angle is cut to follow the radius of the girder between the web and flange and is attached with a single sided 1/4 in. fillet weld. The angles are spaced at 6 feet along the length of the girder. The edge of the angle closest to the end of the beam was 34 in. from the end of the beam. 7/8 in. diameter studs were welded to each flange of the girder at intervals of 6 in. The girder and components were galvanized in accordance with AASHTO M111M/M111.

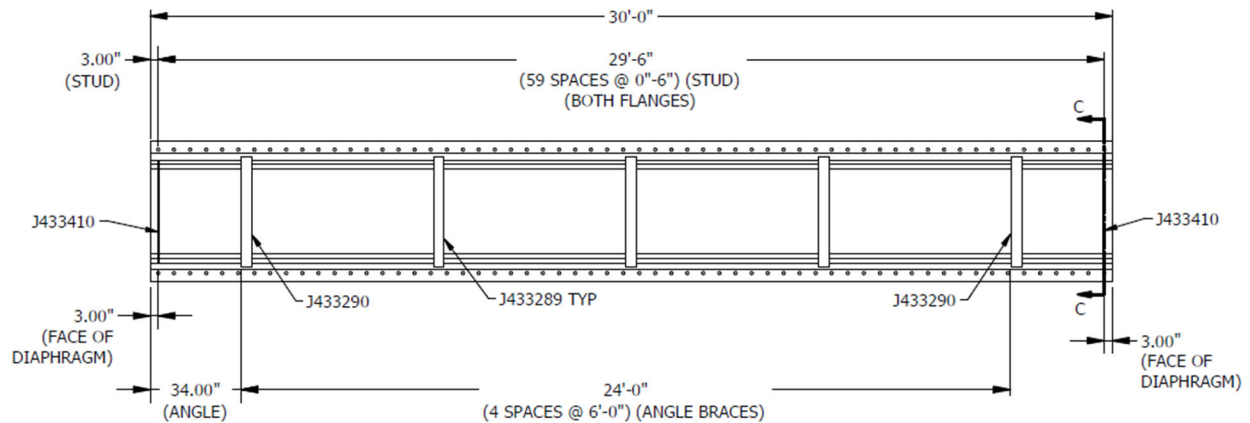


Figure 3 Girder plan dimensions

For the test, each end of the girder was supported on a steel bearing beam that connected directly to the reaction floor. The bearing was a flat surface, ie., no rocker connection was provided, because this type of flat bearing replicates typical field conditions. No positive connection was applied therefore the beam was free to uplift.

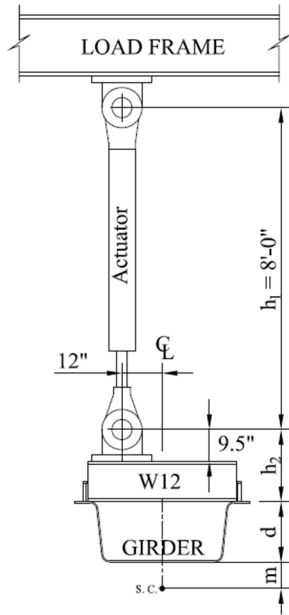
The SIPs used for the test had a 2.0 in. tall rib with ribs spaced at 8.5 in c to c. The thickness of the SIP was 0.030 in. The length of the SIP along the span of the girder, was 34 in and the width of the SIP between the flanges was 44 in. The ends of the flutes have a pre-closed deck end closure condition. To fasten the SIPs to the girder, #12-24 TEK self-tapping screws with a #5 point were used. See the description of each test for fastening pattern.

2.2 Test Procedure

Load for the test was applied through a hydraulic actuator. The hydraulic actuator was attached to a load frame via a swivel that allowed rotation of the actuator transverse to the span of the beam. Load was applied to the girder through a W12 spreader beam. A swivel was bolted to this spreader beam at an eccentricity of 12" and connected to the actuator as shown in Fig. 4.

The specimen was instrumented with a load cell at the actuator to monitor applied load. Extension of the actuator was measured by an LVDT. Additional LVDT's were applied to measure vertical displacement of each flange of the girder. Two LVDT's were applied at the mid-span and two LVDT's at each quarter point of the span. Rotation at mid-span was measured by a precision level applied to the spreader beam. As a check on the mid-span torsion rotation, the rotation at mid-span was calculated by taking the difference between the LVDT readings at midspan and dividing by the horizontal distance between them. There was good correlation between the two methods of determining the mid-span torsional rotation.

Each test was performed by gradually applying load to the girder through the hydraulic actuator in approximate increments of 3 kips up to a maximum force of approximately 15 kips. At each increment, the test was briefly paused while data was recorded. For each test configuration, the girder was loaded fully to the peak load, then unloaded until the actuator force returned to zero. The test was then reperformed, so each specimen was subjected to two cycles.



a) Diagram of the test apparatus

b) Photograph of test frame

Figure 3. Test Eccentric Load Application

A total of eight tests were performed with increasing restraint applied by additional panels and fastening. For Test 1, the girder was tested bare, with no SIPs installed. For Test 2, one SIP was installed at each end of the girder but each SIP was installed with only a single screw at each corner of the panel. For Test 3, three additional screws were added to each flat of the panel for a total of five screws per side of the panel. For Test 4, a second panel was added at each end adjacent to the first panel placed. This panel was attached with a total of five screws per side (one screw in each flat). Where the panels overlapped, the existing screw from the previous panel was left in place and an additional screw was added that penetrated both SIPs. For Test 5, the next panel of SIPs was placed at each end with five screws per side (for a total of 3 SIPs at each end of the beam. For Test 6, the last row of SIPs was installed with five screws per flat on each side of the panel. With this last row of SIPs, the panels covered almost the entire length of the girder, with an approximate 24 in. gap at the mid-span of the girder. For Test 7, the lap of the first to SIP Panels was fastened with five equally spaced screws. This lap coincided with one of the cross angles so the screws penetrated the panels and the leg of the cross angle. For Test 8, the lap between the second and third panel was fastened with five equally spaced screws. This lap did not coincide with an angle so the connection was only between the two panels.

2.3 Test results

The mid-span rotation of the girder versus the applied load is plotted for each test in Fig. 5. For clarity, only the first cycle of each test (part “a” of the two-cycle test) is plotted. Typically, the results of the second cycle (part “b”) closely followed the first cycle. As expected, the greatest rotation (1.85 degrees) is observed for the bare girder with no SIPs attached (Test 1). For Test 2, the attachment of the first SIP provided some resistance to rotation, but because this SIP was only fastened at the corners, the increase in resistance was minimal and the peak rotation was 1.75 degrees. However, in Test 3 with the first SIP panel fully fastened, a greater resistance to torsion

is observed and the peak rotation was reduced to 1.55 degrees. For Test 4, there is an increased resistance to torsion with the peak rotation reduced to 1.3 degrees.

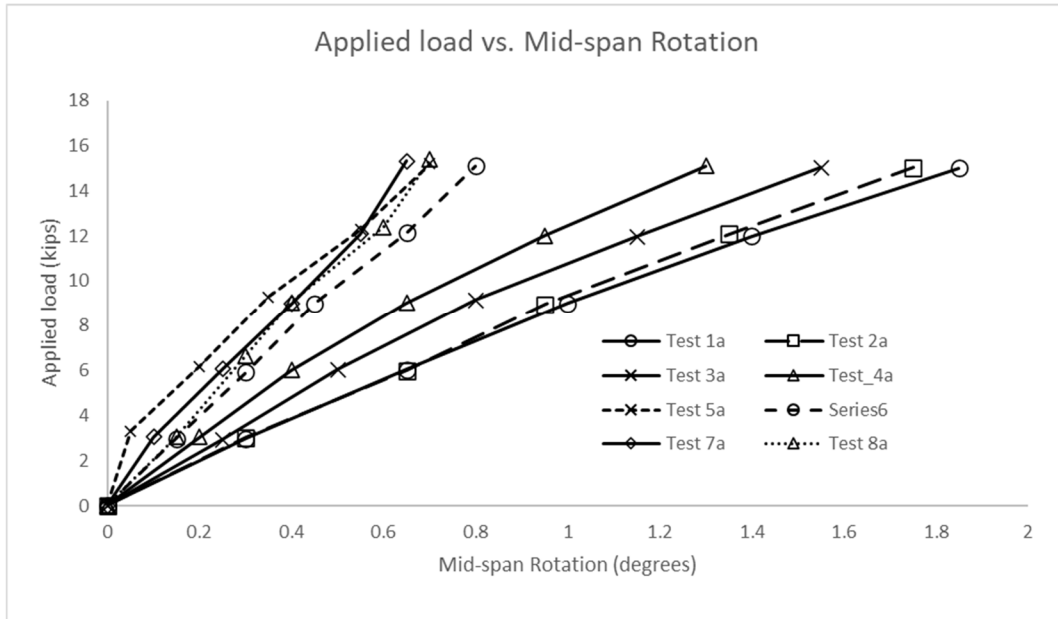


Figure 5 Load versus mid-span torsion rotation plots for all tests

The increased resistance to rotation with the addition of the second panel is slightly less than the increase observed when the first panel was added. This reduction is expected because the resistance of the panels is related to the rate of change of the angle of twist. This rate of change of the angle of twist found as the derivative of the angle of twist relative to position along the length, ϕ' , is greatest at the ends of the girder and reduces to a rate of change of zero at midspan. The rate of change is a function of the span of the girder relative to its warping resistance. The span of the tested girder relative to the warping resistance is small, so the rate of change of the angle of twist is almost constant from the end of the span to the quarter point, then gradually decreases to zero at midspan. More discussion about the relationship of the rate of change of the angle of twist to the resistance of the SIP panels is provided in Section 4.

Tests 1 through 4 show some nonlinear behavior. This non-linear behavior is believed to be a result of geometric nonlinearities in the test. The shear center for the girders is 7.911 in. below the bottom of the girder. Therefore, as the girder rotates about the shear center, the centroid of the girder effectively displaces laterally. As a result of this lateral displacement, the eccentricity of the applied load is increased, effectively increasing the torsional moment applied to the girder as shown in Fig. 6.

There is a significant jump in the torsional response between Test 4 and Test 5 that is not well understood. It is expected that the addition of the third panel for test 5 would result similar reduction in the angle of twist as for the difference between Test 3 and Test 4. Furthermore, the peak angle of twist for Test 5 should also logically be greater than that for Test 6, which has additional SIP panels applied providing additional resistance. Instrumentation errors were ruled out because the measured mid-span deflection is consistent with theory and there is consistency in

the measured rotations between the precision level and the difference of the mid-span LVDT's. A possible explanation is that the entire position of the girder shifted on its end bearings such that there was an angle on the actuator that reduced the eccentricity of the applied load and thus showed less rotation during the test. It is hoped that the ongoing FE element analysis will provide insight into possible sources of this anomaly

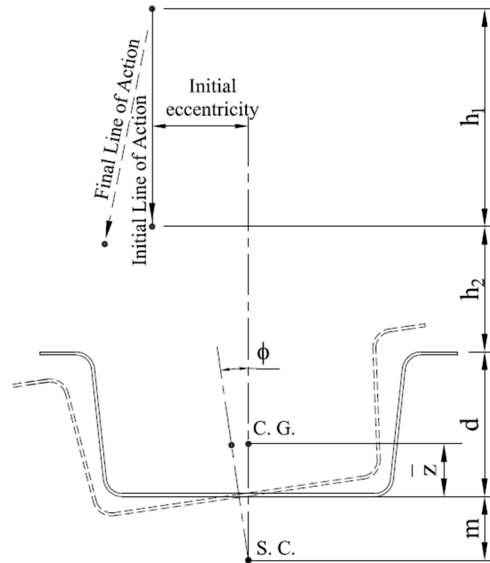


Figure 6 Geometric second order torsion

The peak angle of twist for Test 6 is 0.8 degrees. Based on the theory that the resistance provided by the SIP is related to the rate of change of the angle of twist, it is expected that the reduction in the angle of twist would be less, however these values are reasonably in line. It should be noted that the behavior is closer to linear because as the angle of twist is being reduced, so too are the geometric second order effects

There is a slight increase in the torsional resistance for Test 7 which added side lap fasteners between the first and second set of SIPs. For metal deck used in building systems, the addition of side-lap fasteners can often greatly increase the panel stiffness. In this case, the demands on the end fasteners are relatively reasonable and the warping of the SIP panels is already fairly restrained so the side-lap fasteners only provide a marginal increase in stiffness. Likewise, for Test 8 which added side-lap fasteners between the 2nd and 3rd SIP panel, the addition of these fasteners had an almost negligible increase in the rotational resistance.

3. Finite Element Modelling

To better understand the torsional behavior of the tub girder, a shell finite element model was constructed using SAP2000. The model used linear material behavior but included geometric non-linearities. The model was compared to the results of the tests and showed good correlation.

3.1 Description of the Finite Element Model

The cross-section of the girder was subdivided into segments approximately 2 in. wide. This discretization was chosen so that approximately square elements could be provided with divisions

along the length of the girder at 2 in. Each flange was divided into two elements. The radius between the flange and the web as well as the radius between the web and the bottom of the tub were divided into two elements. Straight elements were used to approximate the radius. Each web was divided into eight elements and the bottom of the tub was divided into sixteen elements. A thin shell element was used for each element for the tub and a linear steel isotropic material with a modulus of elasticity of $E = 29000$ ksi was used.

At 3 in. from the end of the girder, a diaphragm plate is used to stiffen the bearing of the girder. To align the nodes of the tub girder with this plate, the first four rows of elements along the length of the girder had a length of 1.5 in. so that the diaphragm plate could be located at 3 in. from the end and at 6 in. from the end the elements transitioned to a 2 in. (51 mm) length along the member. The plate itself was modeled as a thin shell element comprised of a linear steel isotropic material with $E = 29000$ ksi. This diaphragm plate is connected to the tub via $\frac{1}{4}$ " fillet welds. In the model, the diaphragm plate nodes were directly connected to the tub girder nodes with no reduction in the stiffness of the connection.

The L4x4x $\frac{1}{4}$ cross angles were modeled with two elements for each leg and were discretized into twenty-two elements along the length resulting in elements that were approximately 2 in. square. The top leg of the angle was connected to the top flange of the girder where the fillet radius transitioned to the flange. The vertical leg of the angle followed the approximated curvature of the radius with triangular elements. In initial models of the bare girder, the nodes of the angles were connected directly to the nodes of the tub, but these models showed that the angles were providing unrealistic warping restraint to the torsion deformation. In subsequent models, these joints were separated by 0.1 in. and connected by a linear link element to represent the $\frac{1}{4}$ in. fillet weld connection. The link was assigned an axial stiffness of 100 kip/in. in each of the three coordinate directions. This change in connection stiffness resulted in much better alignment of the model to the test results.

The SIPs were discretized into five elements across the width of the tub and four elements along the length of the tub resulting in approximately 10 in. square elements. The SIPs were connected to the top flange of the girder approximately 1 in. from the fillet radius transition. The elements comprising the flange of the tub which are typically 2 in. by 2 in. were further discretized in this location to 1 in. by 1 in. elements to facilitate this connection. The nodes of the SIPs were offset from the tub elements by 0.1 in. and a linear link element was used to connect the nodes. The link elements were assigned an axial stiffness of 100 kip/in in each direction. Because the SIPs were modeled as a flat plate, adjustments were made to represent the behavior of the ribs. The element used for the SIPs was assigned a membrane thickness of 0.03 in (the actual thickness of the material) and a bending thickness of 0.67 in. to provide an equivalent moment of inertia of the panel of 0.300 in⁴/ft. Based on Ozgur et al (2007) and the correlation of the model to test results, for a fully fastened panel (five fasteners per bearing end), an effective shear modulus of the panel, $G' = 10000$ lb/in was used. For Test 2 where only the corners were fastened, a reduced effective shear modulus $G' = 2000$ lb/in. was modelled based on the test results. The additional screws along the side, while they don't transfer substantial force, limits the out of plane deformation of the panel which can significantly reduce the panel stiffness. To model the diaphragm stiffness, is stiffness, an orthotropic material was used. With this type of material assignment in SAP, the shear modulus of the material, G , can be directly defined. The relationship between the effective shear modulus

of the panel, G' , and the shear modulus of the material is defined by dividing the panel diaphragm stiffness by the thickness of the panel, that is $G = G'/t$.

The shear modulus for the material to provide a diaphragm stiffness of 10,000 lb/in is 333 kip/in². For Test 2, a reduced diaphragm stiffness of 2,000 lb/in and a corresponding shear modulus of 67 kip/in² was used to account for the reduced stiffness of the panel only connected at its corners.

In the tests, load was applied to the girder using a spreader beam. A W12x65 spreader beam was modeled using a frame element between the two flanges of the girder. To represent the offset of the applied load due to the height of the beam and the height of the pivot, an essentially rigid frame element extended vertically from the centerline of the spreader beam to the centerline of the pivot. To represent the actuator, a frame element was used to connect the lower pivot to the upper pivot. This actuator was made essentially rigid for bending but was given a negligible axial stiffness. The top pivot was modelled as pin support. The load applied by the actuator was modelled as a concentrated load along the axis of the actuator at the base connection. This modelling of the load allowed the applied load of the actuator to follow the lateral movement of the girder as it underwent torsional rotation and replicate the geometric second order behavior that was observed in the tests.

The supports at the ends of the girder were modelled as a “gap” link element. This type of link element allows for a compressive only force to represent the bearing type condition of the end supports. The model was run as nonlinear with evaluation of P-delta effects, ie. iteration was performed until equilibrium was achieved on the deformed shape.

3.2 Comparison of Finite Element Results

The finite element model was compared to the results for Tests 1 through 4 with good correlation of the load vs deformation behavior observed. Modelling is still ongoing for Tests 5 through 8. Mid-span vertical deflection was taken as the average of the measurements of the LVDT's measuring the vertical displacement at approximately the midpoint of each flange at mid-span. Similarly, in the FE model, the deflections at the same nodes in the FE model were averaged. This displacement was also compared to linear flexure theory. The mid-span torsional rotation is plotted from two sources of data. The first source is the results provided by the precision level that directly measured angle of rotation at midspan. The second source was the from the displacement measurements of the LVDT's at mid-span. The angle of torsional rotation was calculated based on the difference in the vertical displacement at each of the flanges divided by the distance between the flange center-points. These two sources of data from the test closely aligned. For the FE model, the torsional rotation was determined in the same way as from the LVDT displacements. The test and FE results were also compared to a linear torsion theoretical model that includes both pure torsion and warping torsion rotation components (AISC 1997).

For Test 1, the vertical displacement is shown in Fig 7 a). The FE models shows slightly larger mid-span vertical displacements than the test results which in turn are slightly greater than predicted by flexure theory. Overall, the difference is small (within 10 percent). The difference likely lies in slight differences in the moment of inertia due to the approximated fillets in the FE model as well as some small second order effects due to the slight changes in the geometry as the girder rotates along its length. Overall, the deflection behavior remains linear. The trend in this plot from Test 1 is similar to that of the remaining tests so those plots are not included.

The comparison of the torsional rotation for Test 1 is shown in Fig. 7 b). Both the tests and the FE models show very similar behavior with the tests experiencing slightly larger rotations than that predicted by the finite element models. The non-linear behavior is easy to see when comparing these results to the theoretical linear torsion model. Through the modelling process, it was determined that virtually all of this non-linear behavior is due to the second order effects of the middle of the beam displacing laterally and the corresponding lateral movement of the actuator that increased the torsion applied to the girder.

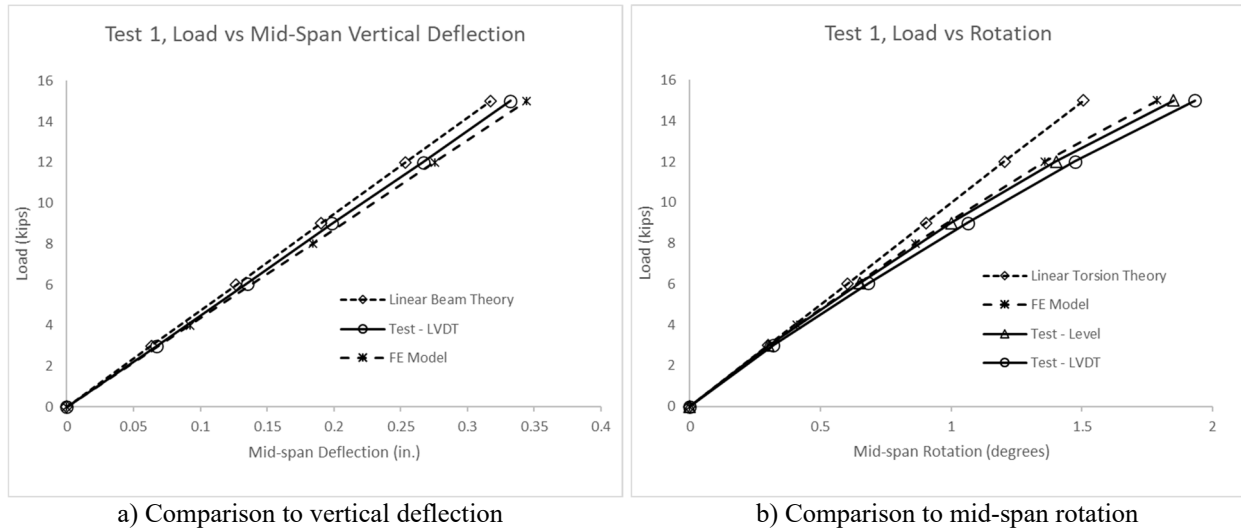
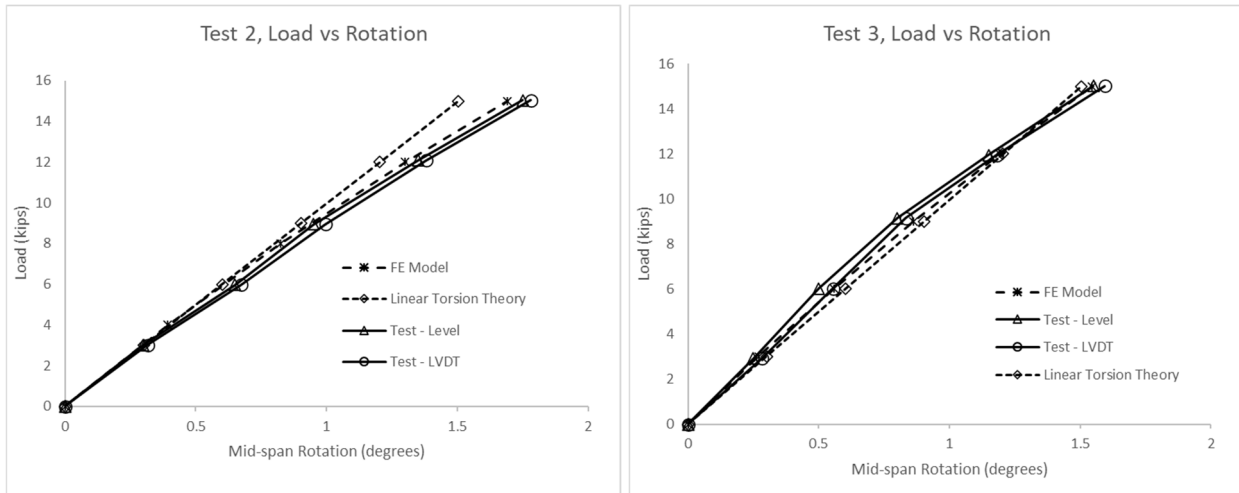


Figure 7 Comparison of FE model to Test 1 results

The FE model torsional rotation comparisons for Tests 2 and 3 are shown in Fig. 8. As with Test 1, the torsional rotation predicted by the FE model closely follows the rotations measured by the test. For Test 2, where the SIP is only connected at the corners, the rotation originally follows the linear torsion theory line, but because the panel only adds minimal restraint, the rotations at higher load levels driven by second order effects exceed the linear theory. For Test 3, when superimposed relative to the linear torsion theory plot, the additional torsional stiffening that the SIP provides can be observed at lower load levels until the second order effects affect the behavior at higher load levels.

The results for Test 4 are shown in Fig. 9. With the addition of the second SIP panel, the rotation of the girder at midspan is reduced relative to a bare girder with no SIPs. Like with the previous tests, the correlation between the test and the FE model is good, however the results from the test indicate the test is initially stiffer and then FE model with good agreement at peak load. A possible explanation for the deviation in behavior could be due to the nonlinear shear behavior of the panels. In the test, the stiffness of the panels may have decreased as the load demand increased so they may actually have a greater stiffness initially than was modeled in the FE model, which was modeled as linear. Tests of the SIP panels are planned to characterize the exact shear behavior of the panels used.



a) Test 2

b) Test 3

Figure 8 Load versus rotation relationship Tests 2 and 3

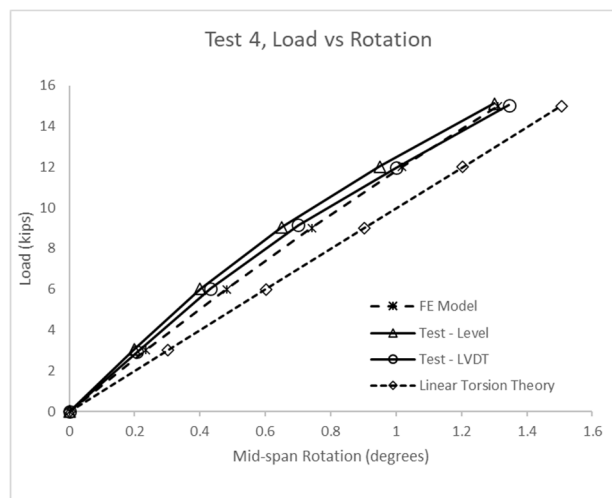


Figure 9 Load versus rotation relationship Test 4

4. Analytical Model

An analytical model was developed to predict the effect that the SIP has on the torsional behavior of the tub girder. By first understanding the interaction between the girder and the SIPs, this will unlock the ability to predict other behavior such as demands on the panel and fasteners, changes in stresses in the girder and ultimately help predict changes in the strength of the member when subjected to torsional loads.

4.1 Defining angle of Twist

To understand the behavior, the deformation of the flanges of the girder at the SIP fastener locations at the ends of the member was observed from the finite element model. The SIP panel was modelled as 46 in. wide and 33 in. along the length of the girder. Fig. 11 a) shows the x (transverse) and y (longitudinal) displacements from the peak load in Test 1 FE model of the corner

nodes where the SIP is to be attached. Initially, it was believed that the restraint provided by the panels would restrain the warping at the end of the beam. The warping deformation would be indicated by large relative displacements in the y-direction between points 1 and 2 (0.0428 in. as well as between 3 and 4 (0.0409 in.). However, these displacements are small compared to the relative displacements in the x-direction between points 1 and 3 (0.2126 in) and points 2 and 4 (0.2115 in), which are a function of the difference in the angle of twist along the length of the girder (from point 1 to point 3).

These relative deformations between points 1 and 3 along the length of the girder can be determined by the difference in the angle of twist, ϕ , of the girder between the two points. For the concentrated torque at mid-span, the angle of twist, ϕ_1 , can be predicted at any location, y , between the end of the beam and mid-span by Eq. 1.

$$\phi_1 = \frac{T_1 L}{GJ} \left(\frac{y}{2L} - \frac{a}{L} \frac{\sinh\left(\frac{y}{a}\right)}{2 \cosh\left(\frac{L}{2a}\right)} \right) \quad (1)$$

where T_1 is the concentrated torque at midspan, L is the span length, G is the shear modulus of the girder, J is the pure torsion constant for the girder, and the torsion term, a , is defined

$$a = \sqrt{\frac{EC_w}{GJ}} \quad (2)$$

In Eq. 2, C_w is the warping constant for the girder and E is the modulus of elasticity.

With the angle of twist defined at any location, y ; using a small displacement approximation, the lateral displacement, Δ_x , of the nodes at the top flange can be approximated by taking the product of the angle of twist at that location, ϕ , and the distance from the shear center to the plane of the SIP. This distance is the sum of the depth of the girder, d , and the distance to the shear center, m , which is below the bottom of the girder as shown in Fig 10. The shear strain, γ , of the girder between different points along its length can be calculated using small angle approximations by dividing the difference in lateral displacement at two points along the length of the girder by the distance between the points as long as that distance is relatively small (as is the length of the SIP panel). The shear force generated in the SIP panels is proportional to the shear strain.

The FE model for Test 3 gives insight into the interaction between the girder and the SIP. The lateral displacements of the top flange nodes, shown in Fig. 11 b) for Test 3 are naturally less than the bare girder from Test 1 due to the restraint provided by the SIP. The forces acting on the SIP connections are shown in Fig. (12a). Because the forces are concentrated at the edges of the panels, the forces can be approximated by opposing couples acting along each edge of the SIP panel Fig. (12b). The shear forces along edge 2 and 4 are summed, and the force along edge 1 and 2 is determined as the force required to balance the couple generated along edges 2 and 4.

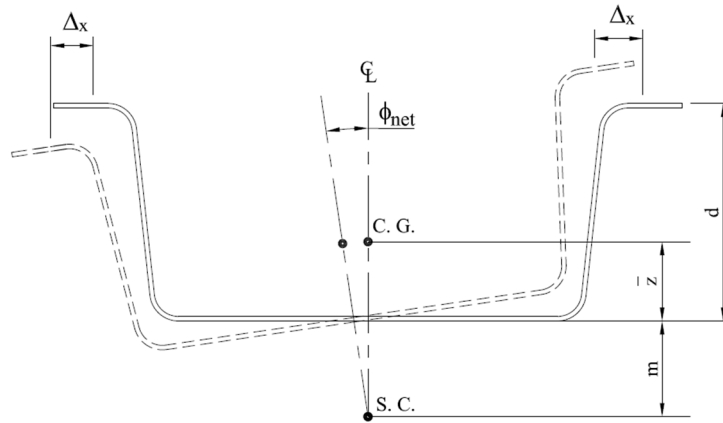
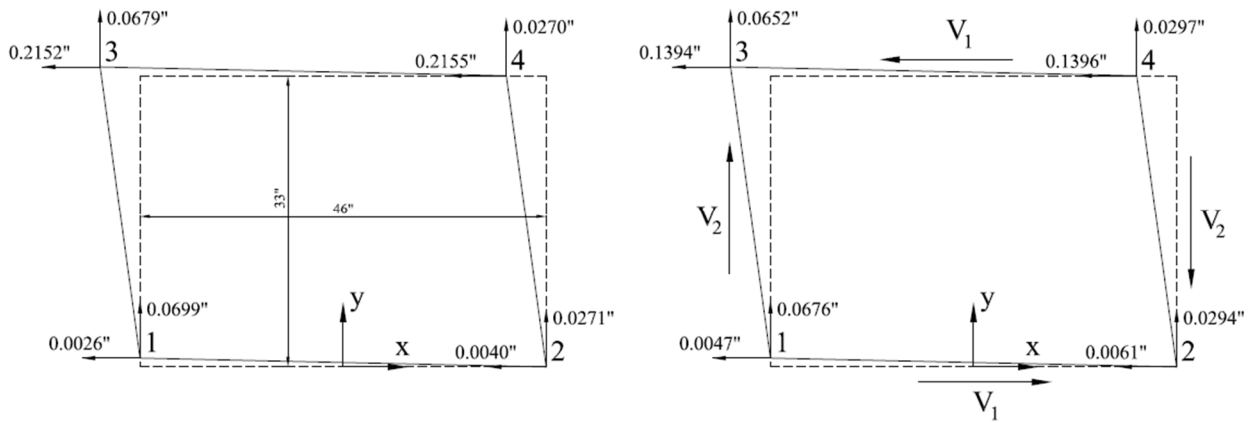


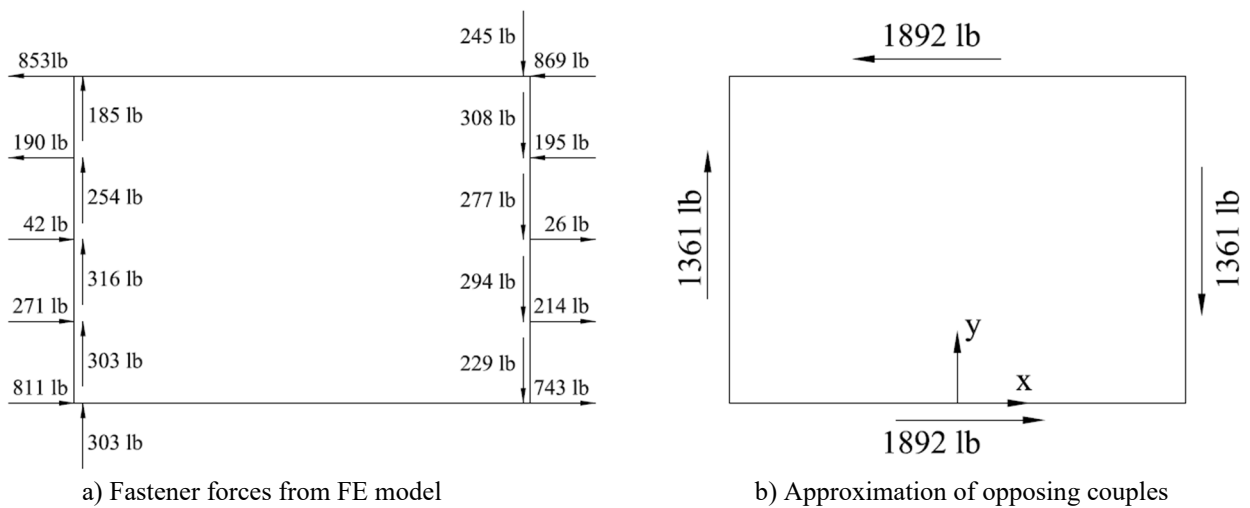
Figure 10 Flange lateral displacement related to angle of rotation



a) Test 1 with no SIP panel

b) Test 3 with one SIP panel

Figure 11 Girder flange displacement for Test 1 and Test 3



a) Fastener forces from FE model

b) Approximation of opposing couples

Figure 12 Forces acting on the SIP panel for Test 3

As additional panels are added, the trend of the shear forces along the panel edges continues. The panels overlap for tests 4-6, but no side-lap fasteners are applied although the panels share a fastener at the corners where they overlap. The panels act as individual shear panels but at the location where the panels overlap, transverse shear forces counter-balance. Thus, the approximation of couples acting along the outside edges of the panels is consistent for the case of multiple panels at the ends of the girder.

Fig. 13 shows the forces exerted on the girder from the panels. These forces create couples such that the panel is equilibrium, so there is no net moment about the vertical z-axis of the girder. However, the forces, V_1 , acting in the x-direction create opposing torsional moments, T_p , at each end of the SIP – one at the support location and the other along the span. This torque acting along the span is the effect that reduces the mid-span rotation of the girder.

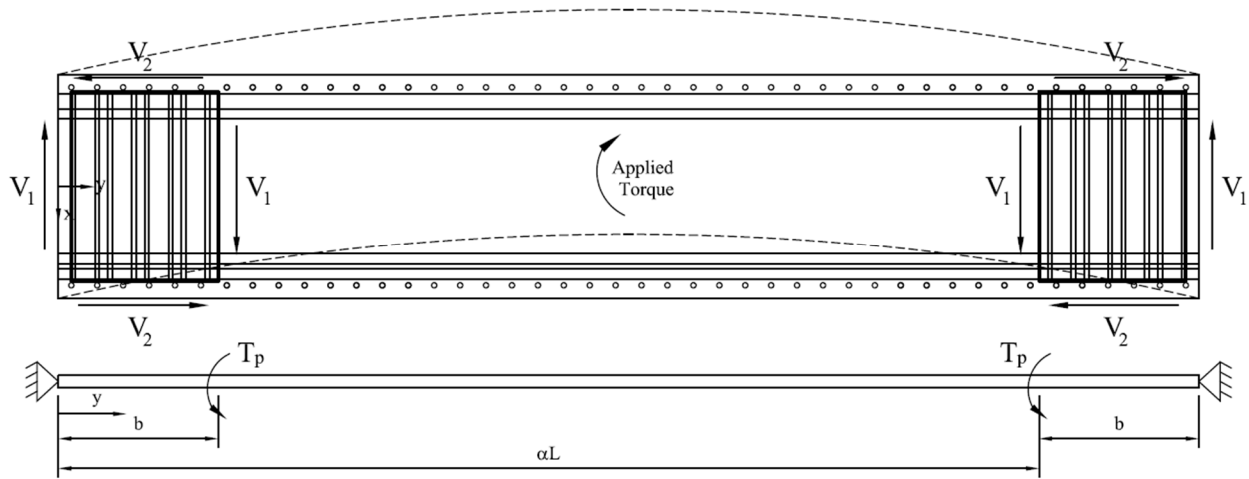


Figure 13 Panel forces acting on girder and corresponding torsion model

The angle of twist, ϕ_2 , caused by the symmetric torsional moments T_p can be defined at any location y between the end of the girder and mid-span by Eq 3.

$$\phi_2 = \frac{T_p L}{GJ} (X1) \quad (3)$$

where

$$X1 = \left((1 - \alpha) + \frac{a}{L} \left(\frac{\sinh\left(\frac{\alpha L}{a}\right)}{\tanh\left(\frac{L}{a}\right)} - \cosh\left(\frac{\alpha L}{a}\right) \right) \left(\sinh\left(\frac{y}{a}\right) + \sinh\left(\frac{L-y}{a}\right) \right) \right) \quad (4)$$

In Eq. 4, $\alpha = 1-b/L$, and b is the distance from girder support location to the end of the SIP panel system, assuming that the SIP system initiates at the end bearing location of the girder.

The forces in the panels, V_1 and V_2 , and the corresponding resisting torque, T_p , are proportional to the net angle of twist, ϕ_{net} at the end of the panel.

$$T_p = \phi_{\text{net}} (d + m)^2 \frac{G'h}{b} \quad (5)$$

The net angle of twist, ϕ_{net} , at the end of the panel is the difference between the angles of twist, $\phi_1 - \phi_2$, defined from Eq. 1 and Eq. 3 respectively with y defined at the end of the panel ($y = b$) in both equations. Eq. 1 and Eq. 3 can be combined to solve directly for the net angle of twist at the end of the SIP panel, ϕ_{net} .

$$\phi_{\text{net}} = \frac{T_1 L}{GJ} \left(\frac{y}{2L} - \frac{a}{L} \frac{\sinh\left(\frac{y}{a}\right)}{2 \cosh\left(\frac{L}{2a}\right)} \right) \left(\frac{1}{1 + \frac{(d+m)^2 G' \cdot h}{b} \cdot \frac{L}{GJ} X1} \right) \quad (6)$$

The term in the last set of parentheses in Eq. 6 is a factor less than or equal to one that quantifies the proportion of the angle of twist is reduced at the end of the panel by the application of the panels.

Once the net rotational torque is defined at the end of the panel, the magnitude of the applied torque at the end of the panel can be determined from Eq. 5. The angle of twist, ϕ , at any location, y , between the end of the girder and midspan may be determined by again taking the difference between the angle of twist ϕ_1 and the angle of twist due to the panel restraint, ϕ_2 , shown simplified in Eq. 7.

$$\phi = \frac{T_1 L}{GJ} \left(\frac{y}{2L} - \frac{a}{L} \frac{\sinh\left(\frac{y}{a}\right)}{2 \cosh\left(\frac{L}{2a}\right)} \right) - \frac{T_p L}{GJ} (X1) \quad (7)$$

In Eq. 7, y is the location between the end of the girder and mid-span at which the location of the angle of twist is desired. The term $X1$ from Eq (4) must be redefined based on the new value of y chosen.

4.2 Second order effects

Because the shear center of the girder is located below the girder, as the girder rotates due to an eccentrically applied load, the center of gravity effectively moves laterally, which introduces second order effects. These second order effects are defined differently depending on whether the applied load is a pure gravity load, or whether the angle of the applied load changes as the girder rotates, as is the case in the tests.

For the case where the applied torque is the result of an eccentrically applied concentrated gravity load, $T_{2\text{nd}}$ can be approximated through iteration by Eq 8.

$$T_{2\text{nd}} = P \cdot \phi (d + m + h_2) \quad (8)$$

In Eq 8, h_2 is the height above the top of the girder at which the gravity load is applied as shown in Fig. 4. The second order torque, T_{2nd} , would be added to the first order applied torque, T_1 , in Eq. 1, Eq. 6 and Eq. 8. The process is iterative until the angle of twist stabilizes.

In the case of the test, the loading was applied by an actuator fixed to a load frame which caused the angle of the actuator to change as the girder displaces laterally, increasing the eccentricity of the load as shown in Fig. 6. This second order effect can be approximated by modifying Eq. 8.

$$T_{2nd} = P \cdot \phi (d + m + h_2) \left(1 + \frac{d + m + h_2}{h_1} \right) \quad (9)$$

The second order torsion predicted by Eq 9 was verified by comparing it the additional torsional reaction at the ends of the girder from the FE model. It should be noted that the second order torsion doesn't include the second order effects introduced as a result of the girders self-weight.

4.3 Analytical model comparisons

Fig. 14 shows the comparison of the analytical model to the results of Test 1 which is the configuration with no restraint provided by the SIPs. From the test, the angle of twist is plotted from both the data as measured by the precision level and as calculated from LVDT displacement measurements. The first comparison is the linear torsion analytical model which shows the initial correlation at low load levels but then deviates from the test results as second order torsion is introduced. The second comparison shows the angle of twist predicted using the approximated second order effects for the eccentrically applied load acting in the gravity direction. The third comparison shows the correlation to the test provided by the analytical model that considers the second order effects due to the changing angle of the actuator. This third comparison shows close correlation to the test, although slightly under-predicts the angle of rotation although the difference is less than 5%.

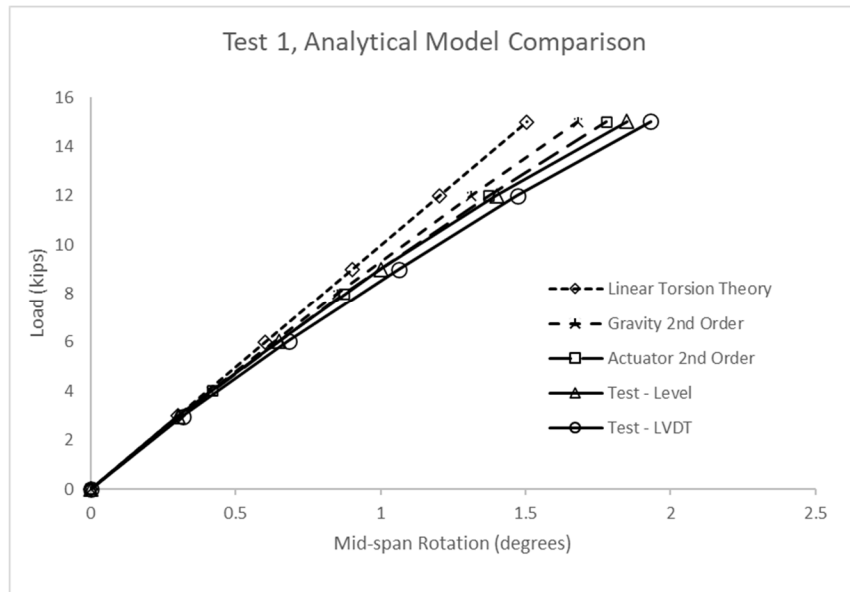


Figure 14 Analytical model comparison to Test 1

Comparisons are made for Test 3 (a single panel fully fastened) and Test 4 (two panels fully fastened) in Fig. 15 and Fig. 16 respectively. These plots show the predicted midspan rotation of the girder without any SIP and the with the respective panels attached relative to measured rotation in the test. In both cases, the analytical model shows good correlation to the test at low load levels with the analytical model prediction slightly less rotation at the at larger load levels.

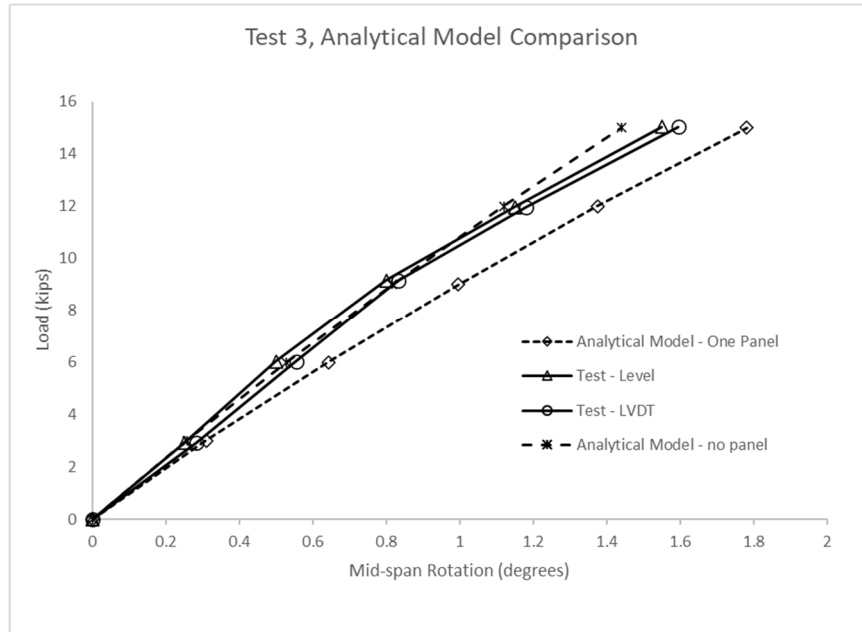


Figure 15 Comparison of analytical model to Test 3

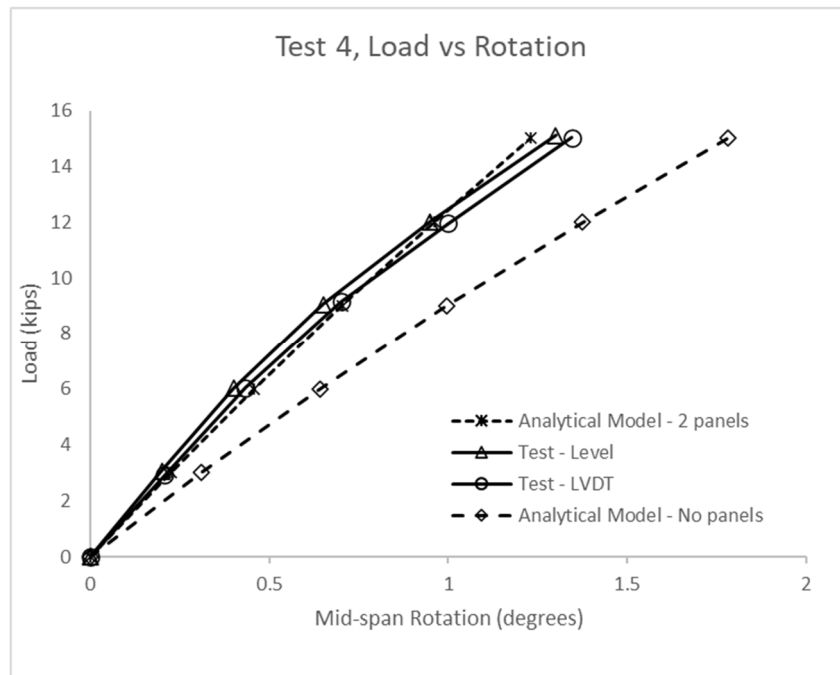


Figure 16 Comparison of analytical model to Test 4

While the plots of Test 3 and 4 in Fig. 15 and Fig. 16 show good correlation between the analytical model and test in terms of the mid-span rotation, there are still some limits in the extent to which the behavior was predicted. Using the finite element results to better understand the behavior, the deformation of the panel and the resulting forces were investigated. The analytical model predicts a larger angle of twist at the end of the panel than the finite element model. Because the forces in the panels are proportional to the angle of twist, the analytical model predicts larger panel forces than the finite element model on the order of 20% to 30%. A deeper investigation into the finite element model behavior indicates that there is localized distortion of the cross section as a result of the concentrated panel shear force being applied laterally to the top flanges. This cross-section distortion shown in Fig. 17 essentially reduces the deformation of the panel and reduces the forces in the panel. Thus, the analytical model will overpredict the restraining forces in the SIP panels. The extent of the distortion is likely to increase as the depth of the girder increases.

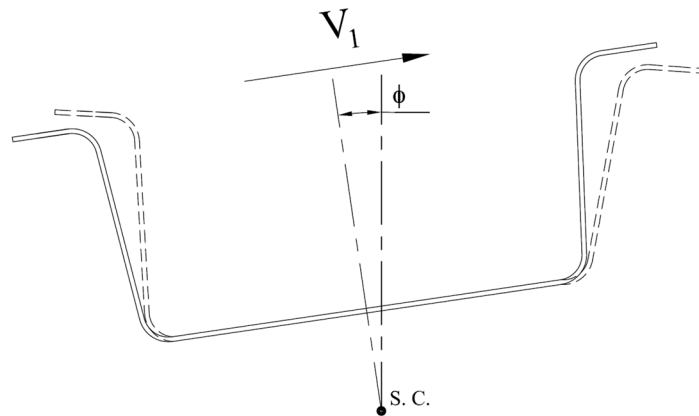


Figure 17 Distortion of cross section from panel forces

5. Conclusions

Tests were performed on press break formed tub girders to measure the response to torsional loading. The girder was initially tested alone, and subsequently tested with increasing number of SIP panels attached between the top flanges of the girder with a total of eight configurations. The attachment of the SIP panels is shown to reduce the torsional rotation of the girder.

A shell finite element model was created to replicate the behavior of the test. The model considered geometric nonlinearities but did not consider any material non-linearities. The finite element models showed good correlation to Tests 1 through 4. Finite element modelling is ongoing for Tests 5 through 8. The second order behavior observed in the tests was determined to be a result of geometric nonlinearities introduced through the application of the test load.

An analytical model was developed to predict the extent to which the attachment of SIP panels restrained the rotation of the tub girder. The analytical model predicts the restraining forces in the panels as a function of the panel effective shear modulus G' . The method also provides an approximation of the geometric second order forces that have a substantial influence on the behavior. The analytical model shows good correlation to Tests 1-4 and analysis is ongoing for Tests 5-8.

Ultimately, the research shows that the addition of SIPs can be effective in reducing the rotation of PBFTGs during construction. The finite element model developed well replicates the torsion behavior and can be considered a starting point for more refined finite element analysis. The analysis can be expanded to larger cross sections and longer spans that are more difficult to test in the lab. Additional modeling can be performed to investigate the study the effects that the restraint provided by the SIP panels have on the buckling behavior of the girders. The analytical model that has been developed distills down the fundamental behavior of the girder related to torsion. While this predicted behavior is specific to the case of a single torsional moment applied at mid-span, the same principles can be applied to other types of loading regimes for routine evaluation of tub girders.

References

- AISC (1997). *Steel Design Guide Series 9: Torsional Analysis of Structural Steel Members*. American Institute of Steel Construction. Chicago, IL.
- Egilmez, O. O., Helwig, T. A., Jetann, C. A., Lowery, R. “Stiffness and Strength of Metal Bridge Deck Forms” *Journal of Bridge Engineering*. 17 (4). [https://doi.org/10.1061/\(ASCE\)BE.1943-5592.0000276](https://doi.org/10.1061/(ASCE)BE.1943-5592.0000276)
- Egilmez, O. O., Helwig, T. A., Herman, R. (2016). “Using Metal Deck Forms for Construction Bracing in Steel Bridges”. *Journal of Bridge Engineering*. 21 (5). [https://doi.org/10.1061/\(ASCE\)BE.1943-5592.0000864](https://doi.org/10.1061/(ASCE)BE.1943-5592.0000864)
- Sanchez, T. A., White, D. W. (2012) “Effects of Stay-in-Place Metal Deck Forms on the Behavior of Steel I-Girder Bridges During Construction. Proceedings of the 2012 World Steel Bridge Symposium, Dallas, TX.
- Valmont (2024). Valmont Press Brake Tub Girder AASHTO Design Guidelines. <https://valmont.showpad.com/share/vn7cYkA3uVkYQ9ZtmAcGE>. Accessed 12/14/2024
- Wang, Y., Moya, S. A., Kintz, J., Helwig, T., Clayton, P., Engelhardt, M. Williamson, E. (2016). “The Impact of Girder Geometry and Bracing Details on the Stability of Steel Tub Girder”, *Proceedings of the Annual Stability Conference*, Structural Stability Research Council, Orlando, FL.